JOURNAL OF VIROLOGY, Sept. 2007, p. 9142–9151 Vol. 81, No. 17
0022-538X/07/$08.00+0 doi:10.1128/JVI.02885-06

DCL4 Targets *Cucumber Mosaic Virus* Satellite RNA at Novel Secondary Structures▽

Quan-Sheng Du,[1,3]† Cheng-Guo Duan,[1,3]† Zhong-Hui Zhang,[2,3]† Yuan-Yuan Fang,[1] Rong-Xiang Fang,[1] Qi Xie,[2] and Hui-Shan Guo[1]*

State Key Laboratory of Plant Genomics, Institute of Microbiology, Chinese Academy of Sciences, Beijing 100101, China[1]; State Key Laboratory of Plant Genomics, Institute of Genetics and Developmental Biology, Chinese Academy of Sciences, Beijing 100101, China,[2] and Graduate University of Chinese Academy of Sciences, Beijing 100049, China[3]

Received 31 December 2006/Accepted 22 June 2007

It has been reported that plant virus-derived small interfering RNAs (vsiRNAs) originated predominantly from structured single-stranded viral RNA of a positive single-stranded RNA virus replicating in the cytoplasm and from the nuclear stem-loop 35S leader RNA of a double-stranded DNA (dsDNA) virus. Increasing lines of evidence have also shown that hierarchical actions of plant Dicer-like (DCL) proteins are required in the biogenesis process of small RNAs, and DCL4 is the primary producer of vsiRNAs. However, the structures of such single-stranded viral RNA that can be recognized by DCLs remain unknown. In an attempt to determine these structures, we have cloned siRNAs derived from the satellite RNA (satRNA) of *Cucumber mosaic virus* (CMV-satRNA) and studied the relationship between satRNA-derived siRNAs (satsiRNAs) and satRNA secondary structure. satsiRNAs were confirmed to be derived from single-stranded satRNA and are primarily 21 (64.7%) or 22 (22%) nucleotides (nt) in length. The most frequently cloned positive-strand satsiRNAs were found to derive from novel hairpins that differ from the structure of known DCL substrates, miRNA and siRNA precursors, which are prevalent stem-loop-shaped or dsRNAs. DCL4 was shown to be the primary producer of satsiRNAs. In the absence of DCL4, only 22-nt satsiRNAs were detected. Our results suggest that DCL4 is capable of accessing flexibly structured single-stranded RNA substrates (preferably T-shaped hairpins) to produce satsiRNAs. This result reveals that viral RNA of diverse structures may stimulate antiviral DCL activities in plant cells.

Endogenous small RNAs associated with RNA silencing pathways, involve the RNase III enzyme Dicer proteins. The activity of the four Dicer-like (DCL) proteins in *Arabidopsis thaliana* on small RNA production has recently been widely investigated through small RNA/*dcl* mutants. DCL1 recognizes the common stem-loop structure of pre-microRNAs (pre-miRNAs) to produce miRNAs (25), DCL2 is responsible for stress-related 24-nucleotide (nt) siRNA production from natural antisense transcripts (4), DCL3 synthesizes 24-nt DNA-repeat-associated siRNAs (ra-siRNAs) that mediate heterochromatin formation (36), and DCL4 processes noncoding RNA into 21-nt *trans*-acting siRNAs (ta-siRNAs) that regulate timing of development and leaf polarity (12, 35, 40). In DCL4 loss-of-function plants (*dcl4* mutant), DCL2 can substitute for the function of DCL4 and generate 22-nt ta-siRNAs (12, 35), revealing the hierarchical redundancy among DCL activities in endogenous ta-siRNA synthesis.

RNA silencing is not only a type of gene regulatory mechanism that is conserved in a broad range of eukaryotes but is also part of a highly adaptable immune system response against foreign RNAs and viruses in plants (1, 8) and animals (7). In plants transformed with an inverted repeat (IR) transgene, DCL4 is required for the production of 21-nt siRNAs induced by IR transgenes that function as cell-to-cell silencing signals (9). Plant virus infection also results in the accumulation of virus-derived siRNAs (vsiRNAs) of 21 to 24 nt in length (14). Increasing lines of evidence have shown that DCL4 is the primary producer of plant RNA 21-nt vsiRNAs in plant antiviral defenses. In *dcl4* mutants, the accumulation of 21-nt vsiRNAs is abolished; instead, 22-nt vsiRNAs with antiviral activities are produced by DCL2 (3, 5, 6, 11). DCL3-dependent 24-nt vsiRNAs are not associated with antiviral defense in RNA virus infections (6) but affect the accumulation of a double-stranded DNA (dsDNA) virus, *Cauliflower mosaic virus* (CaMV) (22). DCL1, which is not involved in RNA virus-derived siRNA production, was recently found to facilitate the production of CaMV 35S leader-derived vsiRNAs of 21, 22, and 24 nt, which requires the combined actions of DCL4, DCL2, and DCL3, respectively, in production (22).

The antiviral role of RNA silencing is further supported by the discovery of many viruses encoding suppressor proteins that interfere with and/or escape from the silencing pathway (20, 34). Based on multiple in vivo and in vitro approaches, increasing evidence suggests that many of the viral suppressors are RNA-binding proteins, either size selective or size independent, though they evolve independently and show low sequence and/or structure homology. Through direct competition target cleavage assays and RNA-induced silencing complex (RISC) formation direct competition assays using *Drosophila* embryo extracts, Lakatos et al. showed that *Tobacco etch virus* HC-Pro, *Tombusvirus* p19, and *Closterovirus* p21 uniformly inhibited siRNA-triggered RISC assembly through sequestering siRNA (17). These findings are strengthened by the

* Corresponding author. Mailing address: State Key Laboratory of Plant Genomics, Institute of Microbiology, Chinese Academy of Sciences, Beijing 100101, China. Phone: 86-010-64847989. Fax: 86-010-64889351. E-mail: guohs@im.ac.cn.

† Q.-S.D., C.-G.D., and Z.-H.Z. contributed equally to this work.

▽ Published ahead of print on 3 July 2007.

three-dimensional structure of p19 (32, 39) and the octameric ring structure of p21 (38). Recently, viral suppressors targeting the key Dicer enzyme (DCL4) or the Argonaute family protein (AGO1), which is the Slicer component of the RISC (2), has also been reported (6, 41). A silencing suppressor, the P38 capsid protein of *Turnip crinkle virus* suppresses DCL4 activity, resulting in the accumulation of a single 22-nt vsiRNA in wild-type *Arabidopsis*, and significantly reduces the IR transgene-derived 21-nt siRNA levels, resembling the siRNA patterns in DCL4-deficient mutants (6). Recently, the 2b suppressor encoded by *Cucumber mosaic virus* (CMV) was shown to inhibit AGO1 cleavage activity in *Arabidopsis*, resulting in increased accumulation of passenger/star strands of small RNAs, both miRNA* and ta-siRNA* (41). The inhibition of AGO1-mediated degradation of star-stranded small RNAs may in turn interfere with the binding of RISC to the complementary target mRNAs guided by siRNAs, consistent with the previous finding that CMV-2b acts downstream of siRNA synthesis and inhibits the activity of long-range silencing signals (13), which is suggested to be siRNA related (9).

It has been shown that vsiRNAs predominantly originate from highly structured single-stranded viral genomic RNAs (23, 31). Very recently, vsiRNAs derived from the dsDNA virus CaMV have been identified as being produced from the branched stem-loop structure within the 35S leader by distinct DCL activities (22). However, the relationship between vsiRNAs and the structures of such single-stranded viral RNA that can be recognized by DCLs has not been investigated yet.

The satellite RNA (satRNA) of CMV (CMV-satRNA) is a 334-nt-long linear RNA with a highly conserved secondary structure and requires helper virus CMV to supply proteins for replication in the cytoplasm (30). Here, we cloned small RNAs derived from the CMV-satRNA and studied the relationship between satRNA-derived small RNAs (satsiRNAs) and the satRNA secondary structure. The definite in vivo models of CMV-satRNA secondary structure were well studied in CMV-infected plants (28). Our results show that satsiRNAs are derived from single-stranded satRNA and DCL4 is the primary contributor of satsiRNAs. The most frequently cloned positive-strand 21-nt satsiRNAs were found to derive from T-shaped hairpins that differ from the prevalent stem-loop-shaped RNAs or dsRNAs which were known as substrates of DCLs to generate miRNAs or siRNA. Our results reveal that DCL4 is capable of accessing flexibly structured single-stranded substrates of invading RNAs to activate an antiviral RNA silencing mechanism in plant cells.

MATERIALS AND METHODS

Plant growth and virus infection assays. *Arabidopsis* wild-type Columbia and *dcl4-2* mutant plants were grown in solid MS medium for 2 weeks and then transferred to soil and grown for 3 weeks under short-day conditions before virus inoculation. Plants were mock inoculated with 5 mM phosphate buffer (pH 7.2) or inoculated with a fresh sap prepared from the ShangDong strain of CMV (SD-CMV)-infected tobacco leaf (1 g of ground leaf material diluted into 2 ml of phosphate buffer). Plant material was collected at 21 days postinoculation for RNA extraction.

Analysis of nucleic acids. Total RNA from *Arabidopsis* was isolated using TRIzol reagent (Invitrogen) according to the manufacturer's instructions, precipitated with isopropanol, and redissolved in 50% formamide. Thirty micrograms of RNA extracted from SD-CMV-infected *A. thaliana* Columbia and the *dcl4-2* mutant were separated by 17% polyacrylamide gel electrophoresis (PAGE) and blotted. Membranes were hybridized with [γ-^{32}P]ATP-labeled DNA oligonucleotide probes complementary to each of the satsiRNA, miR168, miR168*, tasiR255, tasi255*, and miR159, sequences, using T4 polynucleotide kinase (New England Biolabs) or [α-^{32}P]UTP-labeled full-length SD-satRNA transcript (Ambion).

satsiRNA cloning and sequencing. Small RNAs were extracted from SD-CMV-infected *A. thaliana* Columbia at 21 days postinoculation and separated by PAGE in 17% denaturing polyacrylamide gel. RNA fractions with sizes between 18 and 24 nt corresponding to the small RNA population were purified and cloned as described previously (18). The PCR product was directly ligated into pCR2.1-TOPO vector using the TOPO TA cloning kit (Invitrogen). Colonies were screened using PCR. Candidate single colonies were directly submitted for custom sequencing (Sequence Company Sunbio).

RESULTS AND DISCUSSION

CMV-satsiRNAs are asymmetrical in strand polarity. *Arabidopsis thaliana* (ecotype Columbia) were infected with saps extracted from SD-CMV-infected tobacco plants. RNA analysis showed that the SD-CMV-infected *Arabidopsis* plants contained a high level of satRNA (Fig. 1A). We cloned siRNAs from infected *Arabidopsis* plants. Among the 158 randomly sequenced clones, 68 (43%) originated from SD-satRNA (accession no. D89673); some of the small RNAs were cloned two to six times (Table 1). The most common lengths of SD-satRNA-derived siRNAs (satsiRNAs) are 21 (64.7%) and 22 (22%) nt (Fig. 1B). The cloned satsiRNAs corresponded to all regions of the satRNAs in both sense and antisense strands (Fig. 1C); however, asymmetry in strand polarity of satsiRNAs was observed. Forty-two (61.8%) of the total cloned small RNAs were derived from the positive strand, and 26 (38.2%) were derived from the negative strand (Fig. 1C). Some satsiRNA clones had 1 nt insertion or mismatch to the SD-satRNA sequence deposited in the NCBI database. It has been reported that satRNA variants can be generated during the progeny propagation or transmission process of satRNA from one plant species to another—in this case from tobacco to *Arabidopsis* (31). Sequence analysis of SD-satRNA cDNA clones indicated that besides SD-satRNA with the D89673 sequence, two variants were also present in the infected *Arabidopsis* plants (Fig. 1D). Sequence comparison data indicated that the satRNA variants were the source of some satsiRNA clones (Fig. 1D and Table 1).

The 16- to 18-nt small RNAs located at the 3′ end of satRNA (Fig. 1C) were probably by-products of cleavage rather than real DCL products; therefore, they were no longer counted as satsiRNAs. The satsiRNA sequence comparison revealed a hierarchy of nucleotide preference at the first position of small RNAs, with C (42.8%) > U (21.4%) > G (19.0%) > A (16.6%), where there was a strong preference for U at the first position in miRNAs and ta-siRNAs (18; http://asrp.cgrb.oregonstate.edu/db/sRNAdisplay.html). Among the cloned satsiRNAs, three pairs of satsiRNAs were fully complementary in base pairing (Fig. 1C); however, there were no two satsiRNAs able to form a perfect double-stranded duplex with 2-nt overhangs, a feature characteristic of Dicer products derived from dsRNA (10).

The majority of satsiRNAs are derived from single-stranded satRNA. satsiRNAs with different cloning frequency were selected for the confirmation of individual satsiRNA accumulation. All tested satsiRNAs were readily detected by Northern blotting using complementary sequence of corresponding satsiRNAs as probes (referred to as antisense

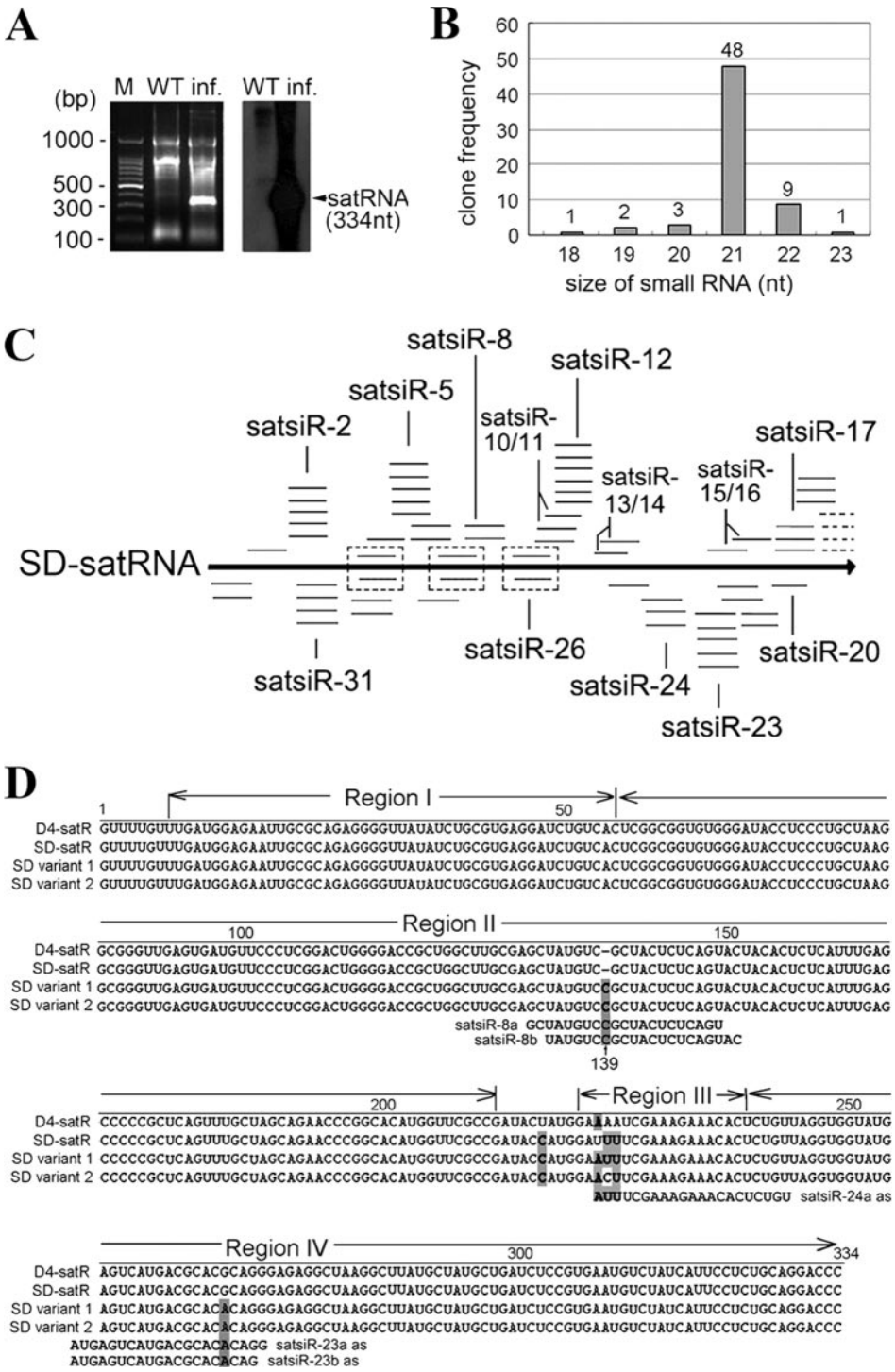

FIG. 1. Origin and characterization of SD-satRNA-derived small RNAs (satsiRNAs). (A) Accumulation of satRNAs in SD-CMV-infected *Arabidopsis*. Total RNA extracted from wild-type (WT) and SD-CMV-infected (inf.) *Arabidopsis* plants was separated in agarose gel and stained with ethidium bromide (left), blotted, and hybridized with an α-^{32}P-labeled probe of SD-satRNA sequence (right). Lane M, molecular size markers. (B) Size distribution of sequenced satsiRNAs. (C) Distribution of satsiRNA clones alongside both strands of SD-satRNA. Small RNAs were aligned with the SD-satRNA genome by sequence comparison. Short lines above the satRNA genome represent satsiRNAs derived from the positive strand, and those below the genome represent satsiRNAs derived from the negative strand. Clone frequencies were represented by the number of short lines at the same position. Small RNAs derived from SD-satRNA variants were also included. The identification serials of some satsiRNAs are indicated. Three pairs of satsiRNAs that were fully complementary in base pairing are boxed with dashes. Four small RNAs located at the 3′ end of satRNA (16 to 18 nt) were not counted as satsiRNAs and are indicated by dashed lines. (D) Alignment of D4-satRNA and SD-satRNA sequences, as well as two SD-satRNA variant sequences obtained from SD-CMV-infected *Arabidopsis* by reverse transcription-PCR and sequencing. Four major folding regions based on the D4-satRNA in vivo structure model are indicated. The C_{139} insertion in SD variants 1 and 2 and sequence heterogeneities are highlighted with dark gray. Some satsiRNA clones identical or perfectly complementary to the SD variants are shown.

TABLE 1. Small RNAs derived from SD-satRNA in SD-CMV-infected *Arabidopsis*

Small RNA[a]	Small RNA sequence[b]	No. of clones	Small RNA length (nt)	Orientation
satsiR-1^{v}	AAGAGGGGUUAUAUCUGCGUG	1	21	+
satsiR-2a	UGAGGA**U**CUGUCACUCGGCGG	2	21	+
satsiR-2b^{v}	UGAGGA**C**CUGUCACUCGGCGG	3	21	+
satsiR-3	CUGCUAAGGCGGGUUGAGUGA	1	21	+
satsiR-4	AGGCGGGUUGAGUGAUGUUCC	1	21	+
satsiR-5a	AGUGAUGUUCCCUCGG-ACUGG	1	21	+
satsiR-5b^{v}	AGUGAUGUUCCCUCGG**U**ACUGG	1	22	+
satsiR-5c	GUGAUGUUCCCUCGG-ACUGG**G**	3	21	+
satsiR-6	UCGGACUGGGGACCGCUGGCU	2	21	+
satsiR-7	CCGCUGGCUUGCGAGCUAUGU	1	21	+
satsiR-8a$^{v1, 2}$	**GC**UAUGUCCGCUACUCUCAGU	1	21	+
satsiR-8b$^{v1, 2}$	UAUGUCCGCUACUCUCAGU**AC**	1	21	+
satsiR-9	CACUCUCAUUUGAGCCCCCGC	1	21	+
satsiR-10a	**G**CCCCCGCUCAGUUUGCUAGC	1	21	+
satsiR-10b	CCCCCGCUCAGUUUGCUAGC**A**	1	21	+
satsiR-11	CGCUCAGUUUGCUAGCAGA	1	19	+
satsiR-12	CAGUUUGCUAGCAGAACCCGGC	6	22	+
satsiR-13	CACAUGGUUCGCCGAUAC	1	18	+
satsiR-14	UGGUUCGCCGAUACCAUGGAU	1	21	+
satsiR-15	AUGACGCACACAGGGAGAGGC	1	21	+
satsiR-16^{v}	CAGGGUAGAGGCUAAGGCUUAUG	1	23	+
satsiR-17a^{v}	**U**GCUGAUCUCCAUGAAUGUCUA	2	22	+
satsiR-17b	GCUGAUCUCCGUGAAUGUCUA	1	21	+
satsiR-18a	**UCCA**UGAAUGUCUAUCAUUCCU	1	22	+
satsiR-18b	CC**G**UGAAUGUCUAUCAUUCCU	1	21	+
satsiR-18c^{v}	C**G**UGAAUGUCUAUCAUUCCU	1	20	+
Small RNA	**CA**UUCCUCUGCAGGACCC	1	18	+
Small RNA	UUCCUCUGCAGGACCC	3	16	+
satsiR-20^{v}	GACAUUCAUGGAGAUCAGC	1	19	−
satsiR-21a^{v}	**U**AGCA-AAGCCUUAGCCUCUCC	1	21	−
satsiR-21b	AGCA**U**AAGCCUUAGCCUCUCC	1	21	−
satsiR-22a^{v}	**G**CCUUAGCC**A**CUCCCUGUGUG	1	21	−
satsiR-22b^{v}	CCUUAGCC**U**CUCCCUGUGUG**CG**	1	22	−
satsiR-23a$^{v1, 2}$	**C**CUGUGUGCGUCAUGACUCAU	3	21	−
satsiR-23b$^{v1, 2}$	CUGUGUGCGUCAUGACUCAU	1	20	−
satsiR-23c^{v}	C-GUGUGCGUCAUGACUCAU**A**	1	20	−
satsiR-24a^{v1}	**A**CAGAGUGUUUCUUUCGAAAU	2	21	−
satsiR-24b^{v}	CAGAGUGUUUCUUUCGAAAU**CC**	1	22	−
satsiR-25^{v}	GAAAUCCAUGGUAUCGGCGAA	1	21	−
satsiR-26	GCGGGGGCUCAAAUGAGAGUG	1	21	−
satsiR-27	ACAUAGCUCGCAAGCCAGCGGU	1	22	−
satsiR-28	UCGCAAGCCAGCGGUCCCCAGU	1	22	−
satsiR-29	UCACUCAACCCGCCUUAGCAG	1	21	−
satsiR-30	CUCAACCCGCCUUAGCAGGGA	2	21	−
satsiR-31a	**C**CACACCGCCGAGUGACAGAUC	1	22	−
satsiR-31b	CACACCGCCGAGUGACAGAUC	3	21	−
satsiR-32	CGCAAUUCUCCAUCAAACAAA	2	21	−

[a] A superscript v indicates the small RNA was derived from a variant (variant 1 or 2).
[b] Different nucleotides of the same or two overlapping satsiRNAs are in boldface.

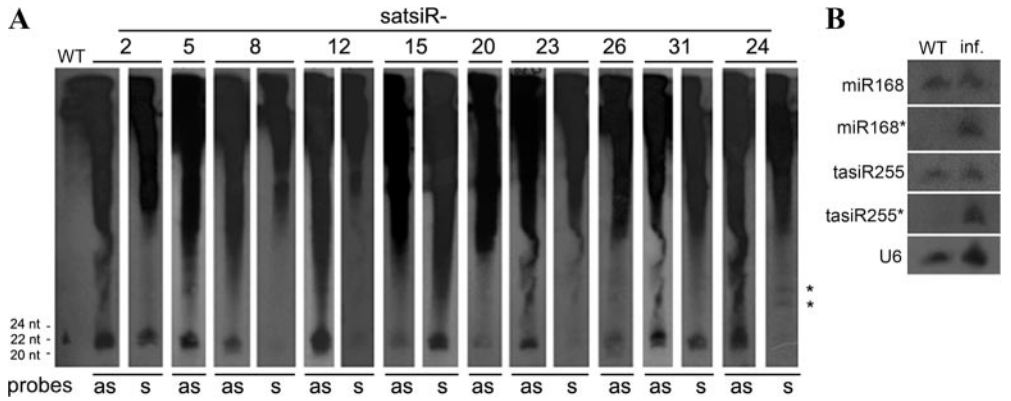

FIG. 2. Detection of small RNAs in SD-CMV-infected plants. (A) Northern blot analysis of representative satsiRNA. Thirty micrograms of small RNA extracted from wild-type (WT) *A. thaliana* Columbia or SD-CMV-infected Columbia was separated by PAGE and blotted. Membranes were hybridized with ^{32}P-labeled probes of specific satsiRNA antisense (as) or sense (s) probes. Two signals detected with the satsiR-24 sense probe corresponding to RNAs larger than satsiRNAs are indicated by asterisks. (B) Accumulation of passenger strands of both miRNA* and tasiRNA* in SD-CMV-infected (inf.) plant. ^{32}P-labeled probe-specific sequences for miR168, miR168*, tasiR255 and tasiR255*, and the U6 control are indicated.

probes) (Fig. 2A). The results showed that the intensity of hybridization signals of satsiRNAs was consistent with their cloning frequency. For example, the most frequently cloned satsiRNAs, satsiR-2, -5, and -12 (cloned five, five, and six times, respectively), showed the strongest signals in Northern blot hybridization, whereas sequences cloned only once (satsiR-15, -20, and -26) had the weakest signals (Fig. 2A and 1C). Moreover, for satsiR-12, besides the 22-nt band, an additional faster-migrating band of 21 nt with lower intensity was also observed. This smaller band might presumably result from hybridization to satsiR-10 and -11, which were 19 to ~21 nt and had 11 or 12 nt of overlap with satsiR-12 (Fig. 1C). However, no clear 19-nt band for satsiR-11 was observed (Fig. 2A), suggesting that the 19-nt satsiR-11 might have missed some nucleotides during the cloning process. Such a possibility was also observed for satsiR-20 and -23b (Table 1), with lengths of 19 nt and 20 nt, respectively, whereas only 21-nt signals were detected by Northern hybridization with the corresponding antisense probes (Fig. 2A).

To detect whether there exists more potential perfect duplexes for cloned satsiRNAs, sequences of some satsiRNAs were used as probes (referred as sense probes) in Northern blot hybridization for further confirmation. Very low or no signal was detected by sense probes of satsiR-8, -12, -23, and -24 (Fig. 2A), consistent with the fact that no opposite-strand sequences of these satsiRNAs were cloned (Fig. 1C). Instead of the expected siRNA band, two large hybridization signals were detected with the satsiR-24 sense probes (Fig. 2A), presumably due to cross-hybridization to satRNA fragments between satsiR-13/14 and satsiR-15/16 (Fig. 1C), as a by-product of satsiRNA production. Signals obtained with satsiR-2 sense probes exhibited features similar to those of the satsiR-31 antisense probes: both detected 21- and 22-nt bands. Correspondingly, the satsiR-31 sense probe and the satsiR-2 antisense probe revealed similar hybridization signals. These data are in agreement with the fact that these satsiRNAs have 17-nt complementary regions (Fig. 1C and 2A and Table 1). The high-intensity signal obtained with the satsiR-15 sense probe (Fig. 2A) was also consistent with the fact that minus-strand-derived satsiR-22 and -23 matched 14 or 15 nt of satsiRNA-15 (Fig. 1C), which was probably responsible for the faint signal revealed with satsiR-23 sense probe (Fig. 2A). In general, Northern blot hybridization using both satsiRNA sense and antisense probes (Fig. 2A) showed good consistency with the satsiRNA cloning results in both size and clone frequency. Together with the fact that the distribution of satsiRNAs covered almost the whole satRNA sequence (Fig. 1C), we speculated that the profile of satsiRNA clones likely represented the population of naturally derived satRNA-related siRNAs in SD-CMV-infected plants.

Recently, Zhang et al. (41) have reported that the accumulation of both miRNA* and passenger strand of a ta-siRNA, siR480/255*, was increased in Fny-CMV-infected and Fan-2b-overexpressing plants. Such accumulation was caused by the CMV 2b protein, a viral suppressor that inhibited the cleavage activity of AGO1 in *Arabidopsis*. Both Fny-CMV and SD-CMV belong to CMV subgroup I; the Fny-2b and SD-2b proteins share 82.9% identity and 86.5% similarity in amino acid sequence. Therefore, we also detected the accumulation of passenger strands of small RNAs in SD-CMV-infected plants. Accumulation of both miR-168* and ta-siR255* was readily detected in SD-CMV-infected plants but not in wild-type strain Columbia plants (Fig. 2B). This result indicated that SD-2b, like Fny-2b, inhibited AGO1 Slicer activity and resulted in stabilizing the passenger strands of small RNAs (41). If satsiRNAs were derived from a satRNA dsRNA replicative intermediate, like dsRNA-derived ta-siRNAs, passenger strands (satsiRNAs*) of perfect double-stranded duplexes should also exist in SD-CMV-infected plants. However, we could not identify any cloned satsiRNAs able to form a perfect double-stranded duplex with 2-nt overhangs (Fig. 1C and Table 1) and, furthermore, the confirmation by Northern blot hybridization with satsiRNA sense probes indicated that satsiRNA* from a perfect duplex did not exist among the satsiRNAs analyzed (Fig. 1C). This suggested that most, if not all, satsiRNAs cloned were not generated from a dsRNA replicative intermediate. It was previously reported that *Cymbidium ringspot tombusvirus* (CymRSV)-derived siRNAs originated predominantly

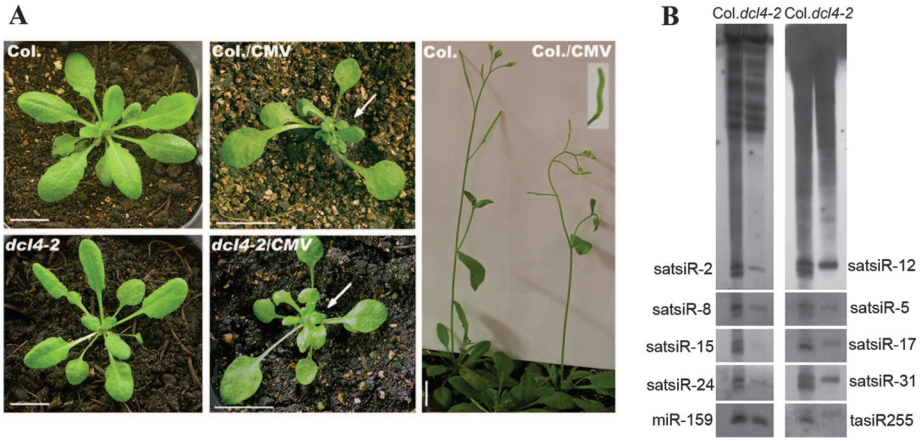

FIG. 3. SD-CMV infection symptoms and accumulation of satsiRNAs in wild-type strain Columbia and the *dcl4-2* mutant. (A) One-month-old wild-type strain Columbia (Col.) and the *dcl4-2* mutant (left two panels). The *dcl4-2* mutant displays downward-curled leaf margins. Ten days post-SD-CMV-infection, wild-type strain Columbia and the *dcl4-2* mutant (middle two panels) show similar developmental defect infection symptoms, which resulted in new leaves fasciated in the center of the plants (arrows). Influorescences of healthy and SD-CMV-infected Columbia strain and the infected snaky siliques (inset) are shown in the right panel. (B) Evidence for the contribution of DCL4 in the production of satsiRNAs. Thirty micrograms of RNA extracted from SD-CMV-infected wild-type strain Columbia and the *dcl4-2* mutant was separated by PAGE and blotted. Membranes were hybridized with ^{32}P-labeled probes specific for each satsiRNA, miR-159, and ta-siR255.

from highly structured single-stranded viral RNA (23). The asymmetry in strand polarity of cloned satsiRNA and failure to detect passenger strand satsiRNA* of the perfectly double-stranded duplex in the presence of CMV 2b suggested that the majority of satsiRNAs cloned are derived from single-stranded satRNA. Like those of most plant RNA viruses, the satRNA negative strand that accumulated during replication is much less abundant than the positive-strand RNA (37). satsiRNAs derived from dsRNA replicative intermediates, if there are any, could therefore be much less abundant than those derived from highly structured positive-strand RNA.

DCL4 is the primary producer of satsiRNAs. DCL4 has been shown to be the major contributor of CMV siRNAs (5, 11) and other 21-nt vsiRNAs (3, 6), as well as CaMV 35S leader-derived 21-nt vsiRNAs (22). We also investigated the activity of DCL4 in satsiRNA synthesis. The similar disease symptoms were observed in wild-type strain Columbia and *dcl4-2* mutants (Fig. 3A): new rosette leaves exhibit developmental defects, including reduced leaf size and a shortened petiole, and finally all new leaves fasciated in the center of the plants and the inflorescence stooped down and crouched with small and snaky siliques. The similar susceptibilities to SD-CMV infection in both wild-type strain Columbia and *dcl4-2* mutants were consistent with the redundant activities among the plant DCLs in mediating antiviral silencing (5, 6, 11). The accumulation pattern of satsiRNAs, however, was altered by the *dcl4* mutation. In the hybridization signals for all tested satsiRNAs, satsiR-2, -5, -8, -12, -15, -17, -24, and -31, the 21-nt satsiRNA bands were abolished in SD-CMV-infected *dcl4-2* plants compared with infected wild-type Columbia strain plants (Fig. 3B). This result indicates that the production of 21-nt satsiRNAs in wild-type plants requires the preferential activity of DCL4. The similar intensity of the 22-nt satsiR-12 hybridization signals detected in wild-type and *dcl4-2* plants suggested that the production of the 22-nt satsiR-12 was not required DCL4. However, the lower-intensity signals of 22-nt bands in *dcl4-2* plants than those in wild-type plants in detection of other satsiRNAs, suggested that DCL4 might have an effect on the production of some 22-nt satsiRNAs (Fig. 3B). Hybridization with the satsiR-17-specific probe showed that the predominant 21-nt satsiR-17 in infected wild-type plants was replaced by a 22-nt species in the infected *dcl4-2* mutants (Fig. 3B). Taken together, our results suggest that satsiRNAs that prevail in wild-type infections mostly derive from certain structures that are specifically accessible by DCL4. Other DCLs, probably DCL2, which can substitute for the function of DCL4 in *dcl4* loss-of-function mutants to produce 22-nt siRNAs, as reported in results of studies of vsiRNA production (5, 6, 11), appear to gain access to satsiRNA precursors in the absence of DCL4.

The most frequently cloned positive-strand satsiRNAs were derived from T-shaped hairpins. The specific role of DCL4 in 21-nt and some 22-nt satsiRNA synthesis and the lack of preference for U at the first position of satsiRNAs suggested that the satRNA substrates recognized by DCL4 differed from endogenous DCL4 dsRNA substrates, which led to the production of endogenous 21-nt ta-siRNAs. This prompted us to examine whether CMV satRNA contains structural features that could be specifically recognized by DCL4 to generate satsiRNAs. We studied the positions of cloned satsiRNAs in the secondary structure of CMV-satRNA (28). There have been three reported structure models of D4-satRNAs, obtained from in vitro transcripts, from total RNA extracted from infected cells (in vivo), or from purified CMV particles (in virion). These structures exhibited slight differences but were identical in most conserved regions (28). It has been proven that these three structure models were valid for all 78 CMV satRNAs analyzed (28). Alignment of SD-satRNA and D4-satRNA sequences shows differences in four residues, U_{217} and $A_{223\text{-}225}$ in D4-satRNA versus C_{217} and $U_{223\text{-}225}$ in SD satRNA, all located within region III (Fig. 1D), which includes a sequence that is highly diverged among all CMV satRNAs (24, 28).

satsiR-2 was found in the highly conserved 5′ end of region

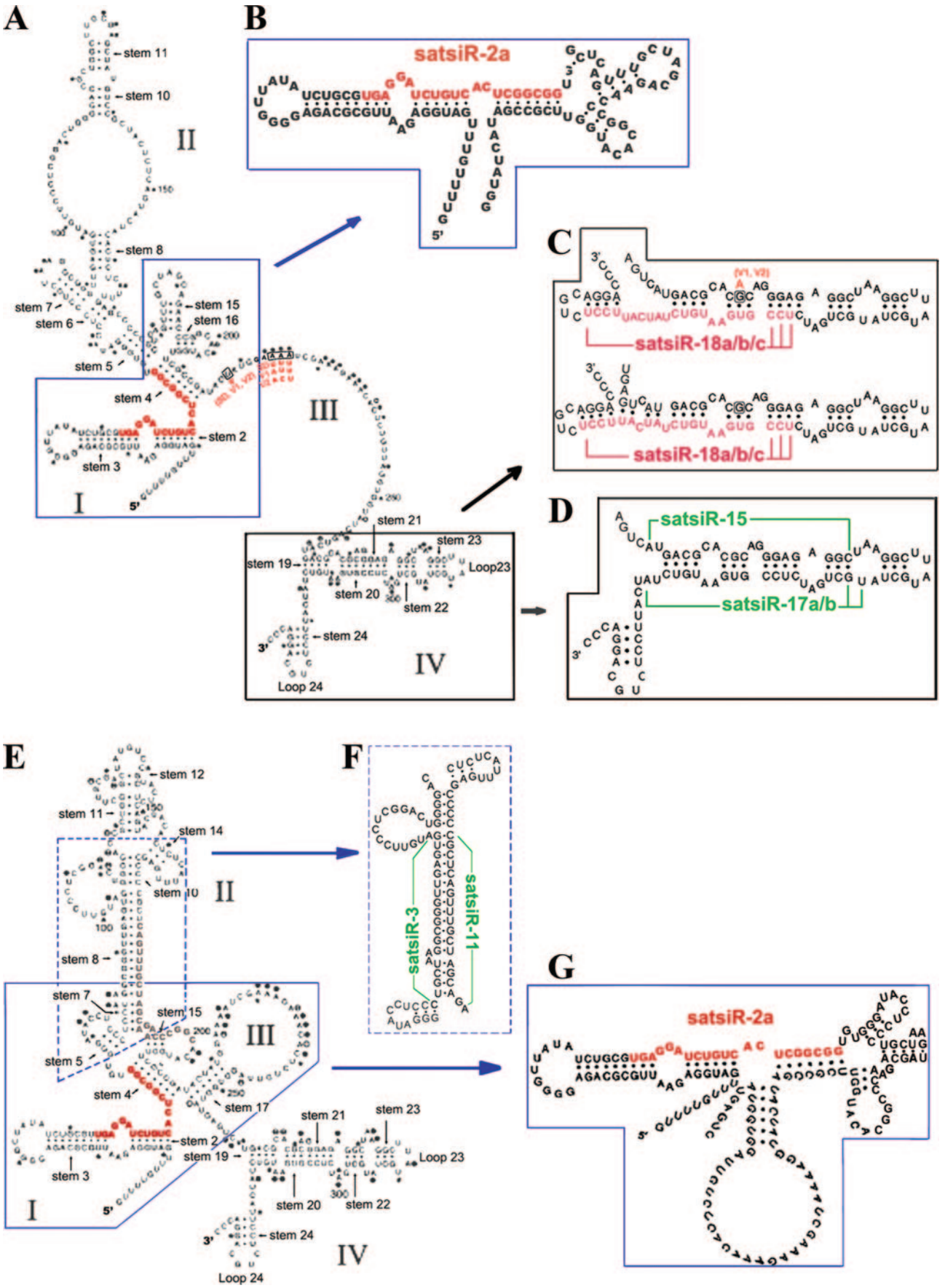
A
B
C
D
E
F
G
satsiR-2a
satsiR-18a/b/c
satsiR-15
satsiR-17a/b
satsiR-3
satsiR-11
stem 2
stem 3
stem 4
stem 5
stem 6
stem 7
stem 8
stem 10
stem 11
stem 12
stem 14
stem 15
stem 16
stem 17
stem 19
stem 20
stem 21
stem 22
stem 23
stem 24
Loop23
Loop 23
Loop 24
I
II
III
IV
5'
3'

I (stems 3 and 2) and extended to the conserved stem 4, which was present in all three CMV satRNA structure models (both in vivo and in virion models are shown in Fig. 4A and 4B, as adapted from Fig. 2A and C in reference 28). The high cloning frequency of satsiR-2 (up to 5 times) and the highly conserved structure in this region suggested that stems 2, 3, and 4 could form a linked unit as a "precursor" hairpin being recognized by DCL4 to produce satsiR-2, which was not produced in the *dcl4* mutants (Fig. 3B), despite the existence of a disconnected sequence that branches off in the satsiR-2 opposite strand (Fig. 4A, B, E, and G). This "precursor," referred as a T-shaped hairpin, differed from the DCL1 recognized stem-loop-shaped miRNA precursors, from which both miRNA and miRNA* sequences were located in the stem region of the hairpin (15, 16, 19, 26, 27), whereas in the T-shaped precursor, only one strand can generate satsiRNAs (Fig. 4B and G).

Such a T-shaped hairpin was also recognized for satsiR-18a/b/c positioned in the highly conserved 3′ end of region IV (Fig. 4C), which was predicted in all three CMV-satRNA structure models covering conserved helices of stems 20, 21, and 24 (Fig. 4A and E).

The findings that both frequently cloned satsiRNAs satsiR-2 and satsiR-18a/b/c were derived from T-shaped hairpins encouraged us to search for a "precursor" hairpin for another abundant satsiRNA, satsiR-5 (cloned up to 5 times). However, no potential stem-loop "precursor" was found in any satRNA structure model (see Fig. 2A, B, and C in reference 28). Unlike the highly conserved regions located at the 5′ and 3′ ends of the satRNA sequence (regions I and IV), region II spanning from nucleotides A_{55} to G_{213} presents different folding structures in the in vitro, in vivo, and in virion satRNA structure models. However, the unconserved structures of region II all possess conserved helices: for example, stems 4, 5, 8, 11, and 14 in all three models and stems 7, 10, and 15 in both in vivo and in vitro structure models (cf. Fig. 2A, B, and C in reference 28). In SD-satRNA variants 1 and 2, there was one nucleotide insertion, C_{139}, in this region (Fig. 1D). We used mFold software to predict the secondary structure of RNA sequences including bases U_{79} to A_{190} of SD-satRNA and its variants (42). No adequate "precursor" hairpin for satsiR-5 sequences was found in any of the four predicted structures for the SD-satRNA sequence. In each predicted structure, the satsiR-5 sequence was partially positioned at the terminal loop end rather than solely in the hairpin stem region (Fig. 5A). In contrast, adequate T-shaped hairpins for satsiR-5 could be recognized in two out of the eight structures predicted for the SD-satRNA variant sequences (Fig. 5B and C, structures 7 and 8). In structure 8, stems 10, 11, and 14 also form a long-stem-loop precursor for satsiR-6 and -8a/b (Fig. 5C). Only satsiR-8a/b containing the C_{139} insertion was cloned in this region. We reason that the insertion of C139 caused the formation of the upper part of the long-stem-loop structure, which resulted in the appearance of T-shaped hairpins for satsiR-5.

In addition to the T-shape-derived satsiRNAs, we also found some satsiRNAs derived from the stem region of imperfect dsRNA duplexes, similar to well-known miRNA precursors. For example, satsiR-15 and -17 might come from an imperfect duplex positioned in the highly conserved 3′-end region IV (Fig. 4D); satsiR-3 and satsiR-11 were found located in the nearly perfectly matched area in region II of the in virion model (Fig. 4F); and satsiR-6 and satsiR-8a were from the long-stem-loop region of the predicted structure 8 (Fig. 5C). The cloning and hybridization results showed that these imperfect stem-loop structures could also be recognized by DCL4 to produce satsiRNAs, (Fig. 3B, satsiR-8, -15, and -17) but were less efficient than the T-shaped structures, indicating that the T-shaped precursor is the primary substrate of DCL4 for CMV satRNA. A previous report has shown that inhibition of AGO1 activity by CMV 2b protein resulted in the accumulation of miRNA passenger strand (41). Similarly, both strands of these potential imperfect duplexes were cloned and detected in SD-CMV-infected plants (Table 1 and Fig. 3B), where both miR-168 and miR-168* were also detected (Fig. 2B). Although the RISC loading process has not yet been investigated in *Arabidopsis*, inhibition of AGO1 Slicer activity by CMV 2b and the resulting accumulation of both miRNA and miRNA* suggested that the loading of miRNA:miRNA* duplexes into AGO1 in plants might share the same properties as that of *Drosophila*, in which siRNA duplexes are loaded into the RISC such that the guide strand of siRNA directs Argonaute-catalyzed cleavage of the passenger strand (21). However, the special structural feature of T-shaped satsiRNA hairpin precursors in which the opposite-strand sequence usually is discontinuous or bulged made it difficult to imagine how such a passenger strand will be accommodated transiently in RISC. The alternative of loading of a single-stranded guide satsiRNA into AGO1 would likely be a process specific to T-shaped structure-derived siRNA in plants, and the passenger siRNA might be degraded by an AGO1-independent mechanism.

Not all plus-strand satsiRNAs could be mapped to long-stem-loop or T-shaped hairpin structures of CMV-satRNA structure models (data not shown), such satsiRNAs might be products of the cleavage of dsRNA paired between the plus and minus strands of satRNA. However, given the high accu-

FIG. 4. Localization of satsiRNAs in in vivo and in virion secondary structure models for CMV satRNA. (A and E) Structure model for D4-satRNA from total RNA extracted from infected cells (in vivo) (A) or from purified CMV particles (in virion) (E) taken from Fig. 2A and C in reference 28. Numbers I, II, III, and IV indicate the four major folding regions. (B) T-shaped hairpin for satsiR-2 (highlighted in red) twisted from the highly conserved 5′-end region I in panel A boxed in blue. (C) T-shaped hairpins for satsiR-18a/b/c (highlighted in purple) twisted from the highly conserved 3′-end region IV in panel A boxed with black lines. (D) Pair of potential imperfect duplex of satsiR-15 and satsiR-17 (indicated with green lines) positioned in the highly conserved 3′-end region IV in panel A boxed with black lines. (F) Pair of potential imperfect duplex of satsiR-3 and satsuR-11 (indicated with green lines) positioned in the nearly perfectly matched area in region II in panel E boxed in blue dashed lines. (G) T-shaped hairpin for satsiR-2 (highlighted in red) twisted from the highly conserved 5′-end region I in panel E boxed in blue lines. The four different residues in region III between D4-satR and SD-satR (SD) as well as mutations detected in the two variants (V1 and V2) are shown in red in panel A. The $G_{269}U$ base pair in D4- and SD-satRNA changed to the AU canonical base pair in the SD-satRNA variants 1 and 2 is shown in red in panel C. (Reprinted from *Virology* (28) with permission of the publisher.)

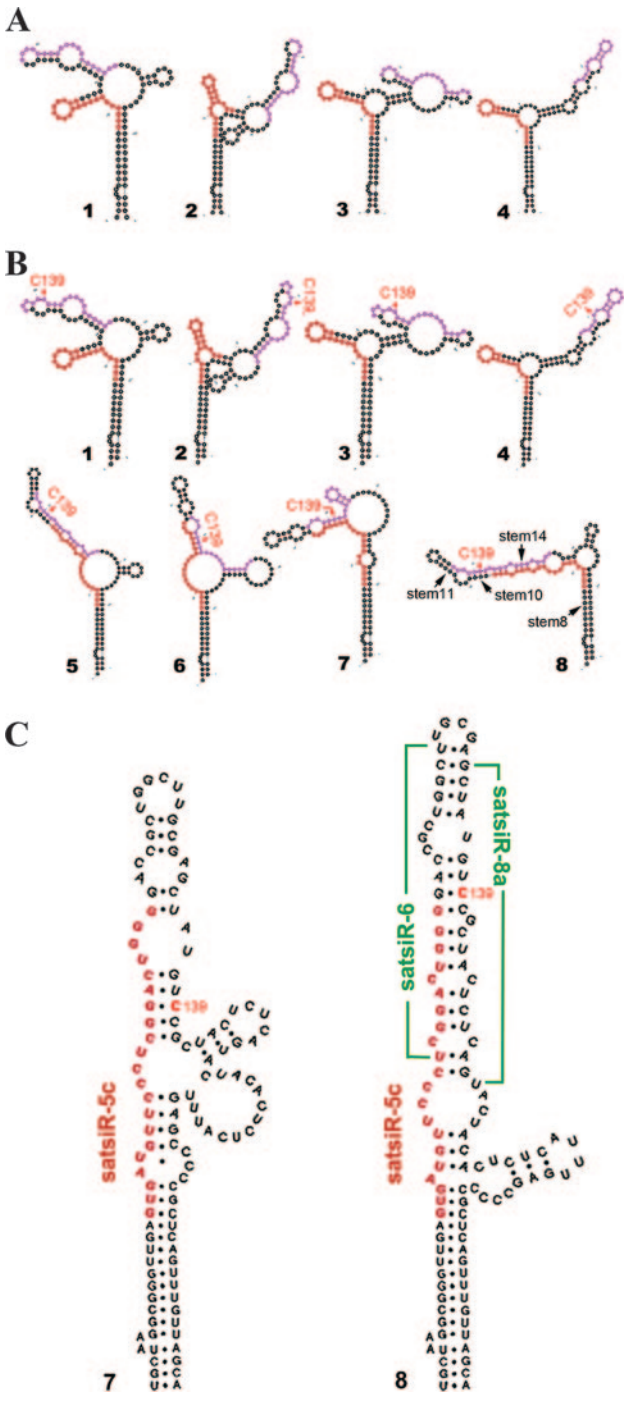

FIG. 5. Predicted T-shaped hairpins for satsiR-5. Secondary structure prediction using the mFold software of RNA sequences including bases U79 to A190 of SD-satRNA (A) and variants with a C_{139} insertion (indicated in red) (B). (A) Four structures for the SD-satRNA sequence. Stem 8 in all of these structures was identical to that of the in virion model of D4-satRNA (see Fig. 4E). (B) Eight structures of SD-satRNA variant sequences. Structures 1 to 4 are similar to those shown for SD-satRNA in panel A. Structures 7 and 8 were twisted as illustrated in panel C to show the adequate T-shaped hairpins for satsiR-5 recognized to position at the upper part of the stem-loop region, and the long-stem-loop precursor for a potential imperfect duplex of satsiR-6 and satsiR-8a is indicated with a green line. Sequences of satsiR-5 and satsiR-8 are highlighted in red and purple, respectively. Stems 10, 11, and 14 formed in structure 8 are indicated.

mulation of satRNAs in CMV-infected plants (Fig. 1A), the possibility that some satRNA molecules acquired different or transient configurations cannot be ruled out. Therefore, specific hairpin "precursors" containing these satsiRNAs recognized by DCL4 might also exist at a certain stage.

Minus-strand satsiRNAs might probably also be derived from highly structured precursors, and such a hypothesis was supported by the analysis of satsiR-24 hybridization results. Minus-strand-derived satsiR-24 is complementary to region III of the CMV-satRNA genome, which contains a large number of adenosine residues, including a single-stranded region with high sequence variability among all CMV satRNAs (24, 28) (Fig. 4A and E). Consistent with this feature, only large hybridization signals were detected with satsiR-24 sense probes (Fig. 2A) and no positive-strand satsiRNAs were cloned in this region (Fig. 1C). This observation strongly suggested that satsiR-24, produced by DCL4 (Fig. 3B), was derived from structured single-minus-strand satRNA.

The above results indicate that most SD-satRNA-derived siRNAs were found in T-shaped or pre-miRNA-like hairpin "precursors" that match highly conserved helix stems of the in vivo secondary structure model of CMV-satRNA. DCL4, which typically recognizes endogenous dsRNA to produce 21-nt ta-siRNAs (12, 35, 40) and IR transgene-derived dsRNA to produce 21-nt siRNAs (9), appears to recognize and cleave diverse partially paired SD-satRNA-derived siRNA precursors formed by single-stranded satRNAs replicating in cytoplasm. The different clone frequencies of satsiRNAs would likely represent the existence of optimal and suboptimal satRNA structures being recognized by DCL4. The fact that the most frequently cloned positive-strand satsiRNAs were derived from T-shaped hairpins supports the idea that such a structure might facilitate a rapid release of DCL4 to make full use of limited resources in plant cells. Our results further support the idea that imperfect intramolecular RNA base pairing, rather than perfect intermolecular RNA base pairing, might strongly stimulate DCL antiviral activities (22). Since there is no other viral genome RNA that has an available structure, the T-shaped or quasi-miRNA hairpin precursors for other vsiRNAs remain to be identified.

On the other hand, the findings of structured single-strand-derived vsiRNAs open a new door into the research of the biochemical nature of pathogen-derived siRNAs in plants. Pathogen-derived siRNAs that are structure dependent rather than by-products of random cleavage of replicative dsRNA intermediates raise the possibility that pathogenicity is the result of the action of these siRNAs on endogenous targets to interfere with host and, in the case of satRNAs, helper virus gene expression (33). About 100 of the host transcripts potentially targeted by CaMV-derived siRNAs have been identified by bioinformatics searches, several of which are effectively down-regulated in CaMV-infected plants (22). By sequence comparisons, we also showed that several satsiRNAs could potentially target *A. thaliana* genome sequences, including some genes encoding transcription factors. Whether these transcription factors and/or other genes are real targets of satsiRNAs and the relationship between satsiRNAs and CMV pathogenicity are currently being investigated. The effect of satRNAs on helper virus-induced symptomatology varies in different virus and satRNA strains and in different host plants,

which indicates the relevance of specific interactions among factors of the three partners (virus, satellite, and host) in the final outcome of the virus infection. The apparent lack of functional open reading frames in CMV-satRNAs (29) raised the possibility that small RNAs derived from satRNA molecules with specific structural and conformational features might exert important biological functions of satRNA in regulation of host and helper virus gene expression.

ACKNOWLEDGMENTS

We thank Juan Antonio Garcia, Nam-Hai Chua, and Shou-Wei Ding for helpful comments and discussions and Juan Antonio Garcia and Xiu-Jie Wang for critical reading of the manuscript. We thank Steven E. Jacobsen for the *dcl4-2* mutant. We thank M. J. Roossinck and G. Alvarado-Rodriguez for the structure of CMV satellite RNA (28).

This research was supported by grants from the National Science Foundation of China (NSFC; grants 30525004 to H.-S.G., 30530500 to R.-X.F., and 30325030 to Q.X.) and by the Ministry of Science and Technology (MOST), China, National Basic Research Program 973 (grant 2006CB101900).

REFERENCES

1. **Baulcombe, D.** 2004. RNA silencing in plants. Nature **431:**356–363.
2. **Baumberger, N., and D. C. Baulcombe.** 2005. Arabidopsis ARGONAUTE1 is an RNA Slicer that selectively recruits microRNAs and short interfering RNAs. Proc. Natl. Acad. Sci. USA **102:**11928–11933.
3. **Blevins, T., R. Rajeswaran, P. V. Shivaprasad, D. Beknazariants, A. S. Ammour, H. S. Park, F. Vazquez, D. Robertson, F. Meins, Jr., T. Hohn, and M. M. Pooggin.** 2006. Four plant Dicers mediate viral small RNA biogenesis and DNA virus induced silencing. Nucleic Acids Res. **34:**6233–6246.
4. **Borsani, O., J. Zhu, P. E. Verslues, R. Sunkar, and J. K. Zhu.** 2005. Endogenous siRNAs derived from a pair of natural cis-antisense transcripts regulate salt tolerance in Arabidopsis. Cell **123:**1279–1291.
5. **Bouche, N., D. Lauressergues, V. Gasciolli, and H. Vaucheret.** 2006. An antagonistic function for Arabidopsis DCL2 in development and a new function for DCL4 in generating viral siRNAs. EMBO J. **25:**3347–3356.
6. **Deleris, A., J. G. Bartolome, J. Bao, K. D. Kasschau, J. C. Carrington, and O. Voinnet.** 2006. Hierarchical action and inhibition of plant Dicer-like proteins in antiviral defense. Science **313:**68–71.
7. **Ding, S. W., H. Li, R. Lu, F. Li, and W. X. Li.** 2004. RNA silencing: a conserved antiviral immunity of plants and animals. Virus Res. **102:**109–115.
8. **Dunoyer, P., and O. Voinnet.** 2005. The complex interplay between plant viruses and host RNA-silencing pathways.Curr. Opin. Plant Biol. **8:**415–423.
9. **Dunoyer, P., C. Himber, and O. Voinnet.** 2005. DICER-LIKE 4 is required for RNA interference and produces the 21-nucleotide small interfering RNA component of the plant cell-to-cell silencing signal. Nat. Genet. **37:**1356–1360.
10. **Elbashir, S. M., W. Lendeckel, and T. Tuschl.** 2001. RNA interference is mediated by 21- and 22-nucleotide RNAs. Genes Dev. **15:**188–200.
11. **Fusaro, A. F., L. Matthew, N. A. Smith, S. J. Curtin, J. D. Hagan, G. A. Ellacott, J. M. Watson, M. B. Wang, C. Brosnan, B. J. Carroll, and P. M. Waterhouse.** 2006. RNA interference-inducing hairpin RNAs in plants act through the viral defence pathway. EMBO Rep. **7:**1168–1175.
12. **Gasciolli, V., A. C. Mallory, D. P. Bartel, and H. Vaucheret.** 2005. Partially redundant functions of Arabidopsis DICER-like enzymes and a role for DCL4 in producing trans-acting siRNAs. Curr. Biol. **15:**1494–1500.
13. **Guo, H. S., and S. W. Ding.** 2002. A viral protein inhibits the long range signaling activity of the gene silencing signal. EMBO J. **21:**398–407.
14. **Hamilton, A. J., and D. C. Baulcombe.** 1999. A species of small antisense RNA in posttranscriptional gene silencing in plants. Science **286:**950–952.
15. **Lagos-Quintana, M., R. Rauhut, W. Lendeckel, and T. Tuschl.** 2001. Identification of novel genes coding for small expressed RNAs. Science **294:**853–858.
16. **Lagos-Quintana, M., R. Rauhut, A. Yalcin, J. Meyer, W. Lendeckel, and T. Tuschl.** 2002. Identification of tissue-specific microRNAs from mouse. Curr. Biol. **12:**735–739.
17. **Lakatos, L., T. Csorba, V. Pantaleo, E. J. Chapman, J. C. Carrington, Y. P. Liu, V. V. Dolja, L. F. Calvino, J. J. Lopez-Moya, and J. Burgyan.** 2006. Small RNA binding is a common strategy to suppress RNA silencing by several viral suppressors. EMBO J. **25:**2768–2780.
18. **Lau, N. C., L. P. Lim, E. G. Weinstein, and D. P. Bartel.** 2001. An abundant class of tiny RNAs with probable regulatory roles in Caenorhabditis elegans. Science **294:**858–862.
19. **Lee, R. C., and V. Ambros.** 2001. An extensive class of small RNAs in Caenorhabditis elegans. Science **294:**862–864.
20. **Li, F., and S. W. Ding.** 2006. Virus counterdefense: diverse strategies for evading the RNA-silencing immunity. Annu. Rev. Microbiol. **60:**503–531.
21. **Matranga, C., Y. Tomari, C. Shin, D. P. Bartel, and P. D. Zamore.** 2005. Passenger-strand cleavage facilitates assembly of siRNA into Ago2-containing RNAi enzyme complexes. Cell **18:**607–620.
22. **Moissiard, G., and O. Voinnet.** 2006. RNA silencing of host transcripts by cauliflower mosaic virus requires coordinated action of the four Arabidopsis Dicer-like proteins. Proc. Natl. Acad. Sci. USA **103:**19593–19598.
23. **Molnar, A., T. Csorba, L. Lakatos, É. Várallyay, C. Lacomme, and J. Burgyán.** 2005. Plant virus-derived small interfering RNAs originate predominantly from highly structured single-stranded viral RNAs. J. Virol. **79:**7812–7818.
24. **Palukaitis, P., and M. J. Roossinck.** 1995. Variation in the hypervariable region of cucumber mosaic virus satellite RNAs is affected by the helper virus and the initial sequence context. Virology **206:**765–768.
25. **Park, W., J. Li, R. Song, J. Messing, and X. Chen.** 2002. CARPEL FACTORY, a Dicer homolog, and HEN1, a novel protein, act in microRNA metabolism in Arabidopsis thaliana. Curr. Biol. **12:**1484–1495.
26. **Pfeffer, S., M. Zavolan, F. A. Grasser, M. Chien, J. J. Russo, J. Ju, B. John, A. J. Enright, D. Marks, C. Sander, and T. Tuschl.** 2004. Identification of virus-encoded microRNAs. Science **304:**734–736.
27. **Reinhart, B. J., E. G. Weinstein, M. W. Rhoades, B. Bartel, and D. P. Bartel.** 2002. MicroRNAs in plants Genes Dev. **16:**1616–1626.
28. **Rodriguez-Alvarado, G., and M. J. Roossinck.** 1997. Structural analysis of a necrogenic strain of cucumber mosaic cucumovirus satellite RNA in planta. Virology **236:**155–166.
29. **Roossinck, M. J.** 2005. Symbiosis versus competition in plant virus evolution. Nat. Rev. Microbiol. **3:**917–924.
30. **Simon, A. E., M. J. Roossinck, and Z. Havelda.** 2004. Plant virus satellite and defective interfering RNAs: new paradigms for a new century. Annu. Rev. Phytopathol. **42:**415–437.
31. **Szittya, G., A. Molnar, D. Silhavy, C. Hornyik, and J. Burgyan.** 2002. Short defective interfering RNAs of tombusviruses are not targeted but trigger post-transcriptional gene silencing against their helper virus. Plant Cell **14:**359–372.
32. **Vargason, J. M., G. Szittya, J. Burgyan, and T. M. Tanaka Hall.** 2003. Size selective recognition of siRNA by an RNA silencing suppressor. Cell **115:**799–811.
33. **Wang, M. B., X. Y. Bian, L. M. Wu, L. X. Liu, N. A. Smith, D. Isenegger, R. M. Wu, C. Masuta, V. B. Vance, J. M. Watson, A. Rezaian, E. S. Dennis, and P. M. Waterhouse.** 2004. On the role of RNA silencing in the pathogenicity and evolution of viroids and viral satellites. Proc. Natl. Acad. Sci. USA **101:**3275–3280.
34. **Xie, Q., and H. S. Guo.** 2006. Systemic antiviral silencing in plants. Virus Res. **118:**1–6.
35. **Xie, Z., E. Allen, A. Wilken, and J. C. Carrington.** 2005. DICER-LIKE 4 functions in trans-acting small interfering RNA biogenesis and vegetative phase change in Arabidopsis thaliana. Proc. Natl. Acad. Sci. USA **102:**12984–12989.
36. **Xie, Z., L. K. Johansen, A. M. Gustafson, K. D. Kasschau, A. D. Lellis, D. Zilberman, S. E. Jacobsen, and J. C. Carrington.** 2004. Genetic and functional diversification of small RNA pathways in plants. PLoS Biol. **2:**E104.
37. **Xu, P., and M. J. Roossinck.** 2000. Cucumber mosaic virus D satellite RNA-induced programmed cell death in tomato. Plant Cell **12:**1079–1092.
38. **Ye, K., and D. J. Patel.** 2005. RNA silencing suppressor p21 of Beet yellows virus forms an RNA binding octameric ring structure. Structure **13:**1375–1384.
39. **Ye, K., L. Malinina, and D. J. Patel.** 2003. Recognition of small interfering RNA by a viral suppressor of RNA silencing. Nature **426:**874–878.
40. **Yoshikawa, M., A. Peragine, M. Y. Park, and R. S. Poethig.** 2005. A pathway for the biogenesis of trans-acting siRNAs in Arabidopsis. Genes Dev. **19:**2164–2175.
41. **Zhang, X., Y. R. Yuan, Y. Pei, S. S. Lin, T. Tuschl, D. J. Patel, and N. H. Chua.** 2006. Cucumber mosaic virus-encoded 2b suppressor inhibits Arabidopsis Argonaute1 cleavage activity to counter plant defense. Genes Dev. **20:**3255–3268.
42. **Zuker, M.** 2003. Mfold web server for nucleic acid folding and hybridization prediction. Nucleic Acids Res. **31:**3406–3415.